

Article

Rosebengal-Loaded Nanoporous Structure Based on Rare Earth Metal-Organic-Framework: Synthesis, Characterization and Photophysical Performance

Kai Song¹, Han Yu¹, Jingyi Zhang¹, Yumeng Bai¹, Yanjun Guan¹, Jingbo Yu¹ and Liqun Guo^{2,*}

¹ School of Life Science, Changchun Normal University, Changchun 130032, China;

songkai@ccsfu.edu.cn (K.S.); y114731@163.com (H.Y.); zjy99323@163.com (J.Z.);

baiyumeng1994@163.com (Y.B.); gyj632122@163.com (Y.G.); yu8trista@163.com (J.Y.)

² School of Life Science, Key laboratory of Straw Biology and Higher Value Application, the Ministry of Education, Jilin Agricultural University, Changchun 130118, China

* Correspondence: guolq948@nenu.edu.cn

Received: 13 February 2020; Accepted: 7 March 2020; Published: 8 March 2020



Abstract: A rosebengal-modified nanoporous structure was designed and constructed. This composite structure consisted of an organic sensitizer based on rosebengal and a supporting host of rare earth metal-organic-framework (MOF). It was identified by means of its x-ray diffraction (XRD) pattern, Infrared (IR) spectra, thermal stability and photophysical measurements. Its absorption was increased by 2,4,6-trinitrophenol. Its rosebengal emission was proportionally increased. But its rare earth emission was well-preserved, offering ratiometric signals. These two sensing modes exhibited linear response and good selectivity with a limit of detection (LOD) of 1.9 μM . Its sensing nature was confirmed as the combination of increased rosebengal emission and rare earth emission quenching effect triggered electron-deficient molecules. This nanoporous structure was superior to traditional ones owing to its double sensing modes.

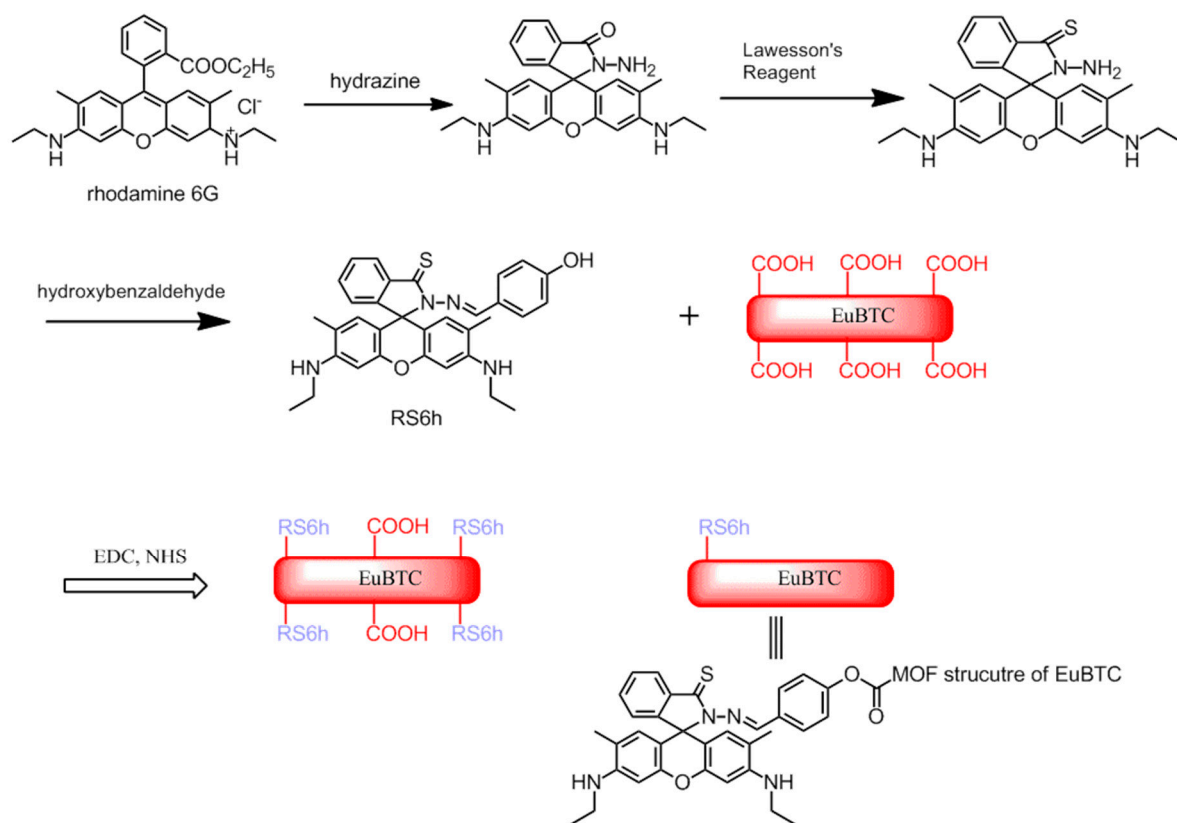
Keywords: 2,4,6-trinitrophenol; nanoporous structure; rosebengal; ratiometric signal

1. Introduction

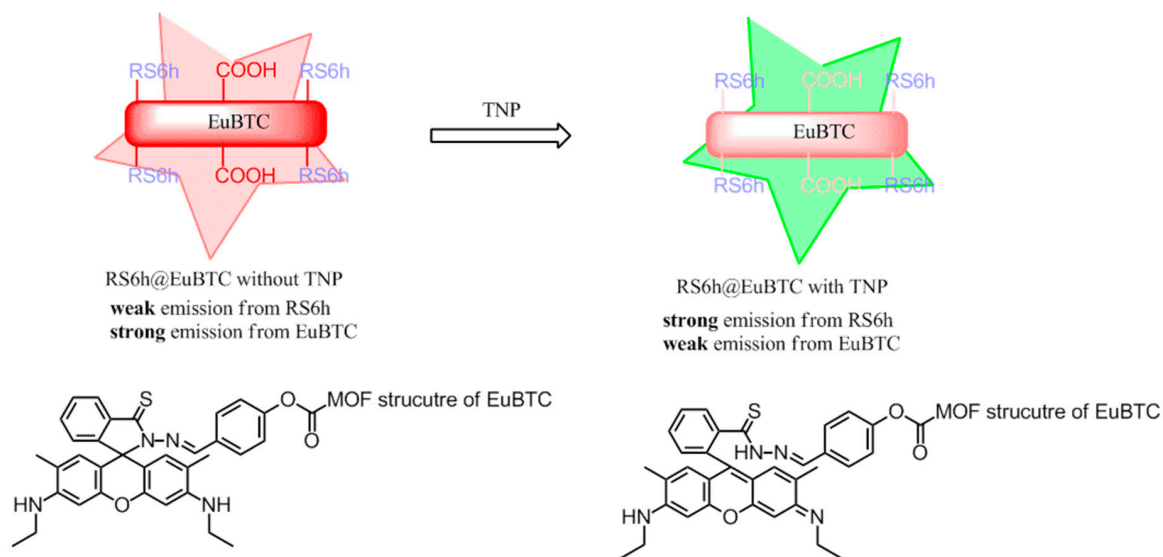
As an explosive and industrial chemical, 2,4,6-trinitrophenol (TNP) has a higher explosion power than 2,4,6-trinitrotoluene (TNT), which makes TNP a threat for public safety [1]. It has been widely-used in manufacturing pigments, antiseptics and pharmaceuticals [2]. Its electron-deficient structure makes it a highly stable one and hard for natural degradation. This feature makes TNP a biohazard pollutant for ecosystems [3,4]. As a result, TNP is a target analyte for public safety, environmental protection and analytical chemistry. There are some reports in the literature that have reported TNP quantification using modern equipment, such as Raman, chromatography and ion mobility [5,6]. These methods, however, need professional pre-treatment, equipment operation and data analysis. They are, thus, not suitable for general-purpose detection. Optical sensing, such as colorimetric sensing and ratiometric sensing, has recently found its application in non-invasive and instant detection, due to its easy operation and limited requirement for instruments [7]. Some literature efforts have confirmed TNP optical recognition [8]. On the other hand, they are generally emission quenching ones, with their emission intensity inversely proportional to TNP concentration. Since emission killers and competing species quench emission as well, selectivity cannot be easily improved. To bypass this issue, probes with emission turn on effect should be developed for TNP. This task, however, is a hard one since the electron-deficient structure makes TNP an efficient emission killer. Alternative proposals should be developed.

As a porous platform, metal-organic frameworks (MOFs) have been recently tried in various fields such as optical sensing, adsorption, catalysis and delivery [9–11]. These MOFs are even modified with organic sensitizers. The resulting hybrid structure emit multiple emission peaks. Some of them are sensitive to analyte identity but the others are not. In this case, ratiometric signals are thus observed with good precision and selectivity. No reference or auxiliary reference will be needed, simplifying sensing operation [12,13].

A hybrid structure is designed in this work, using an organic sensitizer based on rose bengal and a supporting host of rare earth MOF. This dye-MOF hybrid structure is denoted as RS6h@EuBTC. Its construction strategy is depicted in Schemes 1 and 2. Its characterization and performance will be reported herein.



Scheme 1. The construction strategy for RS6h@EuBTC.



Scheme 2. The working strategy of RS6h@EuBTC for TNP.

2. Experimental Brief

2.1. General Information

For the whole synthesis of RS6h@EuBTC, commercially available reagents with AR grade were used with no further purification, such as rhodamine, absolute hydrazine (97%), 1,3,5-benzenetricarboxylic acid (H₃BTC), 1-ethyl-3-(3-dimethylaminopropyl)carbodiimide hydrochloride (EDC), N-hydroxysuccinimide (NHS), Eu(NO₃)₃, Lawesson's reagent and 4-hydroxybenzaldehyde. The characterization of samples was accomplished using a Varian INOVA 300 spectrometer (NMR, Varian, CA, USA), a Agilent 1100 MS spectrometer (MS, Agilent, CA, USA), a Bruker Vertex 70 FTIR spectrometer (IR, Bruker, Baltimore, USA), a Rigaku X-ray diffractometer ($\lambda = 1.5418 \text{ \AA}$) (XRD, Rigaku, Tokyo Akishima, Japan) and a Hitachi S-4800 microscope (SEM, Hitachi, Tokyo, Japan), respectively. Absorption, emission and excitation spectra were measured with a HP 8453 UV-Vis-NIR diode array spectrophotometer (HP, CA, USA) and a Hitachi F-7000 fluorescence spectrophotometer (Hitachi, Tokyo, Japan), respectively. Emission lifetimes were determined through a Lecroy Wave Runner 6100 Digital Oscilloscope (Lecroy, New York, USA) with a Continuum Sunlite OPO excitation source and a FL980 fluorescence lifetime spectrometer (Continuum, West Newton, USA) with a hydrogen flash lamp excitation source.

2.2. Synthesis of Sensing Probe Precursor RS6h

(E)-3',6'-bis(ethylamino)-2-((4-hydroxybenzylidene)amino)-2',7'-dimethylspiro[isoindoline-1,9'-xanthene]-3-thione (RS6h) was synthesized as follows [14]. First, a mixture of rhodamine 6G (5 g), hydrazine (10 mL) and ethanol (20 mL) was heated and stirred under a N₂ atmosphere for 10 h at 85 °C. After vaporizing solvent and excess hydrazine under reduced pressure, the raw product was purified in ethanol/water (V/V = 5:5) to give rhodamine hydrazine. ¹H NMR (CDCl₃), δ (ppm): 1.24–1.25 (t, $J = 6.9 \text{ Hz}$, 6H, NCH₂CH₃), 1.97 (s, 6H, xanthene-CH₃), 3.27–3.29 (q, $J = 6.9 \text{ Hz}$, 4H, NCH₂CH₃), 4.79 (s, N-NH₂), 5.44 (s, NHCH₂CH₃), 6.18 (s, 2H, xanthene-H), 6.49 (s, 2H, xanthene-H), 7.21 (d, $J = 5.6 \text{ Hz}$, 1H, Ar-H), 7.57 (dd, $J = 8.8 \text{ Hz}$, 2.4 Hz, 2H, Ar-H), 8.26 (d, $J = 3.2 \text{ Hz}$, 1H, Ar-H). MS m/z : [M]⁺ calc. for C₂₆H₂₈N₄O₂, 428.2; found, 428.3.

The obtained rhodamine hydrazine was modified with Lawesson's reagent as follows [15]. A mixture of rhodamine hydrazine (10 mmol), Lawesson's reagent (11 mmol) and toluene (30 mL) was heated and stirred under a N₂ atmosphere for 10 h at 125 °C. After removing solvent under reduced pressure, the raw product was purified on a silica gel column with CH₂Cl₂ as an eluent to

give sulfur modified rhodamine hydrazine. ^1H NMR (CDCl_3), $\delta(\text{ppm})$: 1.22–1.24 (t, $J = 6.9$ Hz, 6H, NCH_2CH_3), 1.93 (s, 6H, xanthene- CH_3), 3.24–3.26 (q, $J = 7.1$ Hz, 4H, NCH_2CH_3), 4.75 (s, N- NH_2), 5.40 (s, NHCH_2CH_3), 6.14 (s, 2H, xanthene-H), 6.45 (s, 2H, xanthene-H), 7.17 (d, $J = 5.4$ Hz, 1H, Ar-H), 7.51 (dd, $J = 8.8$ Hz, 2.4 Hz, 2H, Ar-H), 8.24 (d, $J = 3.2$ Hz, 1H, Ar-H). MS m/z : $[\text{M}]^+$ calc. for $\text{C}_{26}\text{H}_{28}\text{N}_4\text{OS}$, 444.2; found, 444.3.

Finally, a mixture of the above obtained sulfur modified rhodamine hydrazine (5 mmol), 4-hydroxybenzaldehyde (5.5 mmol) and ethanol (20 mL) was heated and stirred under N_2 atmosphere for 10 h at 85 °C. After removing solvent under reduced pressure, the raw product was purified on a silica gel column with CH_2Cl_2 as the eluent to give RS6h. ^1H NMR (CDCl_3), $\delta(\text{ppm})$: 1.14–1.17 (t, $J = 7.1$ Hz, 6H, NCH_2CH_3), 1.86 (s, 6H, xanthene- CH_3), 3.14–3.17 (q, $J = 7.4$ Hz, 4H, NCH_2CH_3), 5.31 (s, NHCH_2CH_3), 6.09 (s, 1H, Ar-H), 6.21 (d, $J = 2.4$ Hz, 1H, Ar-H), 6.33 (s, 2H, xanthene-H), 6.40 (d, $J = 0.5$ Hz, 1H, Ar-H), 6.54 (s, 2H, xanthene-H), 7.27 (d, $J = 2.4$ Hz, 1H, Ar-H), 7.39 (d, $J = 1.8$ Hz, 1H, Ar-H), 7.54 (dd, $J = 8.8$ Hz, 2.4 Hz, 2H, Ar-H), 8.23 (d, $J = 3.2$ Hz, 1H, Ar-H), 8.35 (s, 1H, $\text{CH}=\text{N}$), 11.21 (s, Ar-OH). ESI-MS m/e : calc. for $\text{C}_{33}\text{H}_{32}\text{N}_4\text{O}_2\text{S}$, 548.2; found, 548.3 $[\text{M}]^+$.

2.3. Fabrication of Supporting Platform EuBTC

Rare earth supporting platform EuBTC was obtained as follows [15]. A mixture of $\text{Eu}(\text{NO}_3)_3$ (5.0 mmol), NaAc (15.0 mmol) and deionized water (50 mL) was stirred in an ultrasonic bath for 30 min. Ethanol (50 mL) containing H_3BTC (5.0 mmol) was added dropwise into the above mixture. This final solution was stirred under ambient condition for 2 h. The raw product was collected and dried to give EuBTC. Elemental analysis, C: 22.92, N: 0.14, H: 3.13. IR (KBr): 1106 cm^{-1} , 1379 cm^{-1} , 1432 cm^{-1} , 1555 cm^{-1} , 1617 cm^{-1} . Its structure is further confirmed by its XRD curve, which will be discussed below.

2.4. Synthesis of the Dye-MOF Hybrid Structure RS6h@EuBTC

RS6h@EuBTC was obtained as follows [16]. A mixture of EuBTC (1.0 mmol), ethanol (50 mL), EDC (2.0 mmol) and NHS (2.0 mmol) was stirred at ambient condition for 30 min. Then RS6h (2.0 mmol) was dissolved in DMF (10 mL) and added dropwise. This final solution was stirred under ambient condition for 30 h. Solid sample was collected and dried as RS6h@EuBTC. Elemental analysis, C: 32.53, N: 1.52, H: 3.87. IR (KBr): 1012 cm^{-1} , 1112 cm^{-1} , 1220 cm^{-1} , 1271 cm^{-1} , 1370 cm^{-1} , 1432 cm^{-1} , 1520 cm^{-1} , 1555 cm^{-1} , 1608 cm^{-1} , 1696 cm^{-1} , 2967 cm^{-1} . Its structure is further confirmed by its XRD curve which will be discussed below.

2.5. Photophysical Measurement Details

For photophysical spectra collection, EuBTC and RS6h@EuBTC were dispersed in ethanol (0.1 mg/mL) and treated with ultrasonic bath for 1 min. The resulting solutions were poured into quartz cuvettes. Emission spectra were obtained under optimal excitation wavelength determined by excitation spectrum, with optical slit of 0.25×0.25 .

3. Results and Discussion

3.1. Characterization

3.1.1. Micromorphology and Crystal Lattice

A visual understanding can be gained by the SEM images of RS6h@EuBTC and EuBTC shown in Figure 1. Rod-shaped nanocrystals are observed, indicating an optimal orientation for crystal growth. Their mean width and mean length are determined (by a traditional method of calculating pixels and comparing them with scale bar) as ~ 70 nm, and ~ 1.4 μm , respectively. These nanorods are similar to other rare earth MOFs, with average grain size of 36.5 nm calculated by Scherrer formula [15]. Similar distribution and morphology are observed for RS6h@EuBTC nanocrystals. Corresponding average grain size is well preserved (36.2 nm). This observation suggests that modifying EuBTC with RS6h

molecules has a negligible effect on its crystal structure. There are, however, some short nanorods (~400 nm). A more orderless and random distribution is observed for RS6h@EuBTC nanocrystals. The probe loading procedure may break long rods into short ones, decreasing crystal regularity.

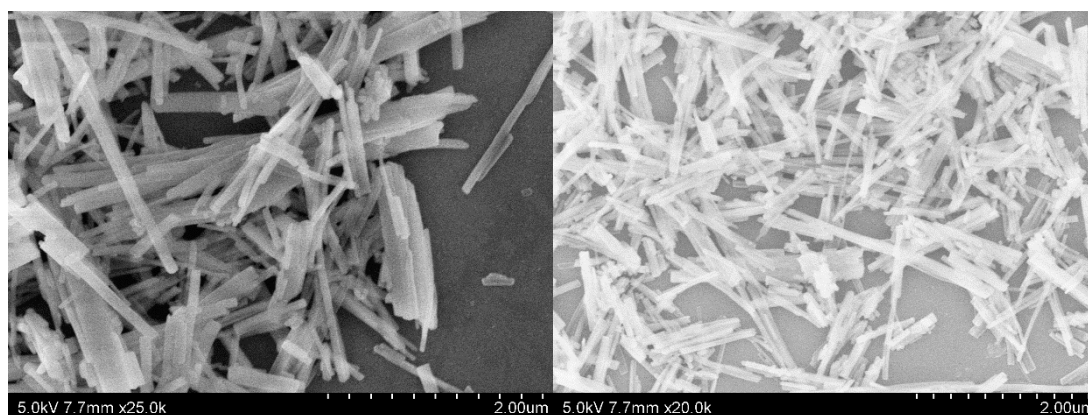


Figure 1. SEM images of EuBTC (left) and RS6h@EuBTC (right).

XRD patterns of RS6h@EuBTC and EuBTC are compared in Figure 2. Both samples show nearly identical 2θ peaks from 8° to 40° , confirming their identical crystal structure. These 2θ peaks are nearly the same as those of $\text{La}(\text{BTC})\cdot 6\text{H}_2\text{O}$ (CCDC 290771). It is, thus, confirmed that $\text{La}(\text{BTC})\cdot 6\text{H}_2\text{O}$, RS6h@EuBTC and EuBTC share the same crystal lattice. In other words, modifying EuBTC with RS6h molecules has a negligible effect on its crystal structure. However, the diffraction intensity of RS6h@EuBTC is weaker than that of EuBTC, particularly within the 2θ region higher than 30° . This is due to the decreased crystal regularity of RS6h@EuBTC.

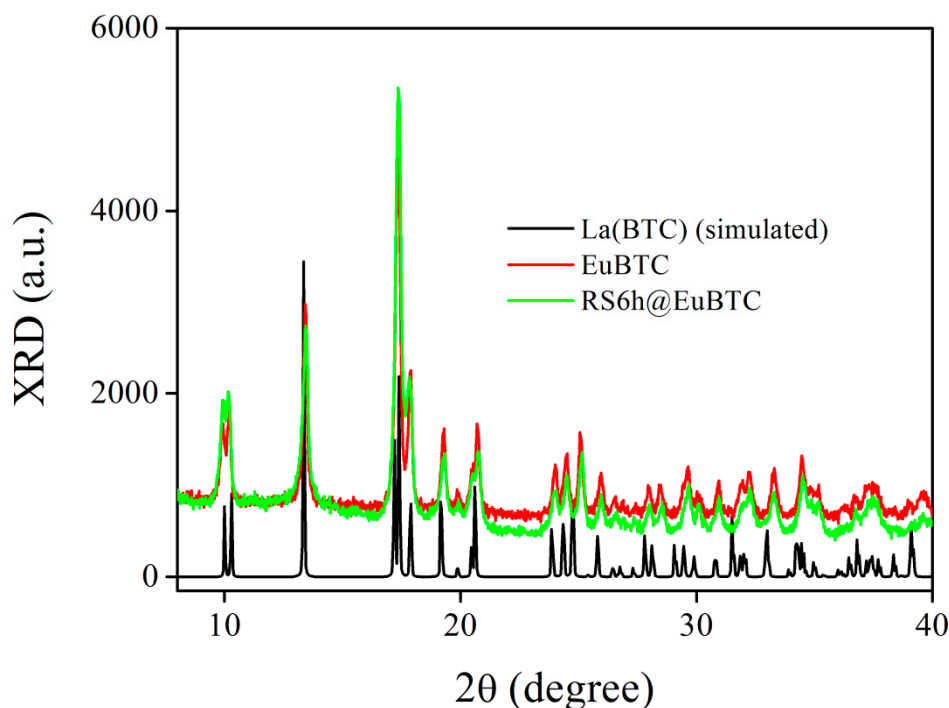


Figure 2. XRD curves of $\text{La}(\text{BTC})\cdot 6\text{H}_2\text{O}$, RS6h@EuBTC and EuBTC.

3.1.2. IR, TGA and Elemental Analysis

The immobilization of RS6h onto EuBTC is confirmed by IR spectra of EuBTC, RS6h@EuBTC and RS6h shown in Figure 3. EuBTC depicts a few characteristic IR peaks centering at 1106 cm^{-1} , 1379 cm^{-1} ,

1432 cm^{-1} , 1555 cm^{-1} , 1617 cm^{-1} , respectively. They are sequentially attributed to the C=O stretching vibration, stretching vibration and bending vibration of dangling –COOH at the EuBTC surface, and the symmetric and asymmetric bending vibration of C=O, respectively [16]. As for RS6h, more IR peaks are detected, centred at 1005 cm^{-1} , 1273 cm^{-1} , 1520 cm^{-1} , 1699 cm^{-1} , 2985 cm^{-1} , respectively. The first one belongs to the C=O stretching vibration. While –NHEt stretching vibration is responsible for the IR band at 1273 cm^{-1} . C=N stretching vibration and C=O symmetric bending vibration correspond to IR bands at 1520 cm^{-1} and 1699 cm^{-1} . The IR band around 2985 cm^{-1} belongs to a –(CH₂)– stretching vibration. RS6h@EuBTC has shown IR characteristics from its two structural components, RS6h and EuBTC. Their wavelength and assignment are listed as follows: 1012 cm^{-1} (RS6h, stretching C=O), 1112 cm^{-1} (EuBTC, stretching C=O), 1220 cm^{-1} (RS6h, stretching –NHEt), 1271 cm^{-1} (RS6h, stretching –NHEt), 1370 cm^{-1} (EuBTC, stretching –COOH), 1432 cm^{-1} (EuBTC, stretching –COOH), 1520 cm^{-1} (RS6h, symmetric bending C=O), 1555 cm^{-1} (EuBTC, symmetric bending C=O), 1608 cm^{-1} (EuBTC, asymmetric bending C=O), 1696 cm^{-1} (RS6h, symmetric bending C=O), 2967 cm^{-1} (RS6h, stretching –(CH₂)–). Slight spectral shift was observed, compared to related ones from EuBTC and RS6h. This is because of the close contact between EuBTC and RS6H, which slightly changes the vibrational energy of these chemical bonds. RS6h@EuBTC shows an IR peak centering at 1220 cm^{-1} which does not belong to RS6h and EuBTC. This IR peak is assigned as the –C–O–C– (ester) stretching vibration, which provides proof for the covalent immobilization of RS6h onto EuBTC.

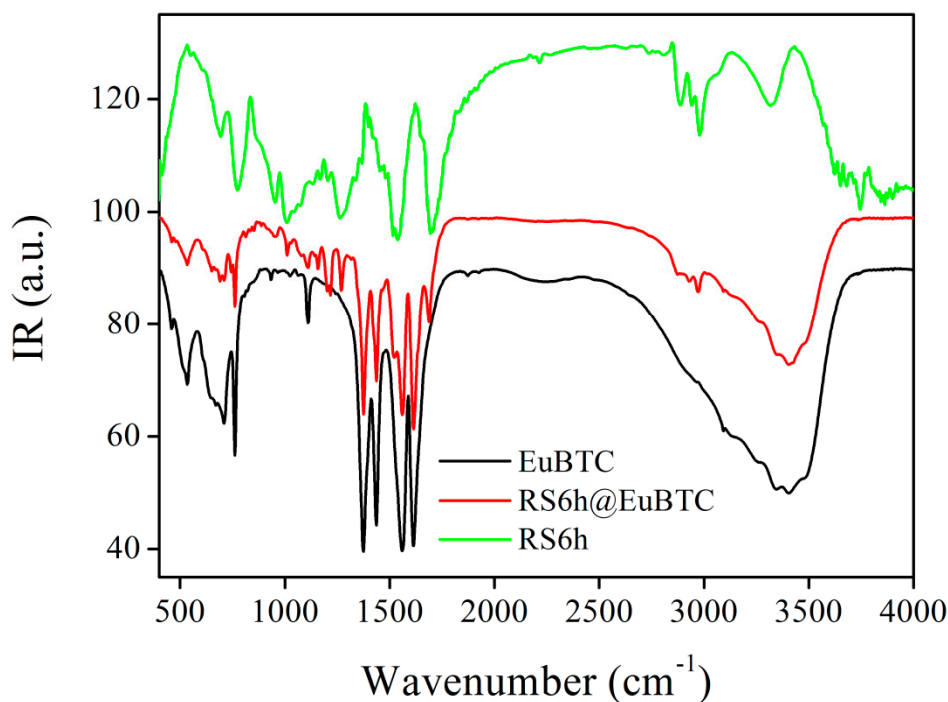


Figure 3. IR spectra of EuBTC, RS6h@EuBTC and RS6h.

RS6h@EuBTC's TGA (thermogravimetric analysis) curve is shown in Figure 4. As indicated by the DTG (derivative thermogravimetry) curve, two obvious weight loss peaks and a minor one are detected. The first one (56–123 °C) shows weight loss of 19.9%. Its sharp endothermic process peaks at 93.5 °C. This weight loss and endothermic temperature are consistent with those of crystal water in EuBTC·6H₂O (23.1%, ~100 °C). The first weight loss is, thus, the thermal evaporation of crystal water from the EuBTC. The following weight loss (288–373 °C) is only 2%. Considering this high endothermic temperature, it is the thermal release of physisorbed molecules in the porous structure of RS6h@EuBTC. An obvious endothermic region is observed (411–493 °C), with weight loss of 34.0%. Considering the obvious weight loss and high endothermic temperature, it is the thermal decomposition of EuBTC framework. Upon even higher temperatures, no obvious weight loss is observed. This whole TGA

curve contains no weight loss originated from thermal evaporation of free RS6h. The above mentioned IR result has confirmed the formation of $-C-O-C-$ bond in an ester group. It is thus confirmed that RS6h molecules have been covalently immobilized onto EuBTC.

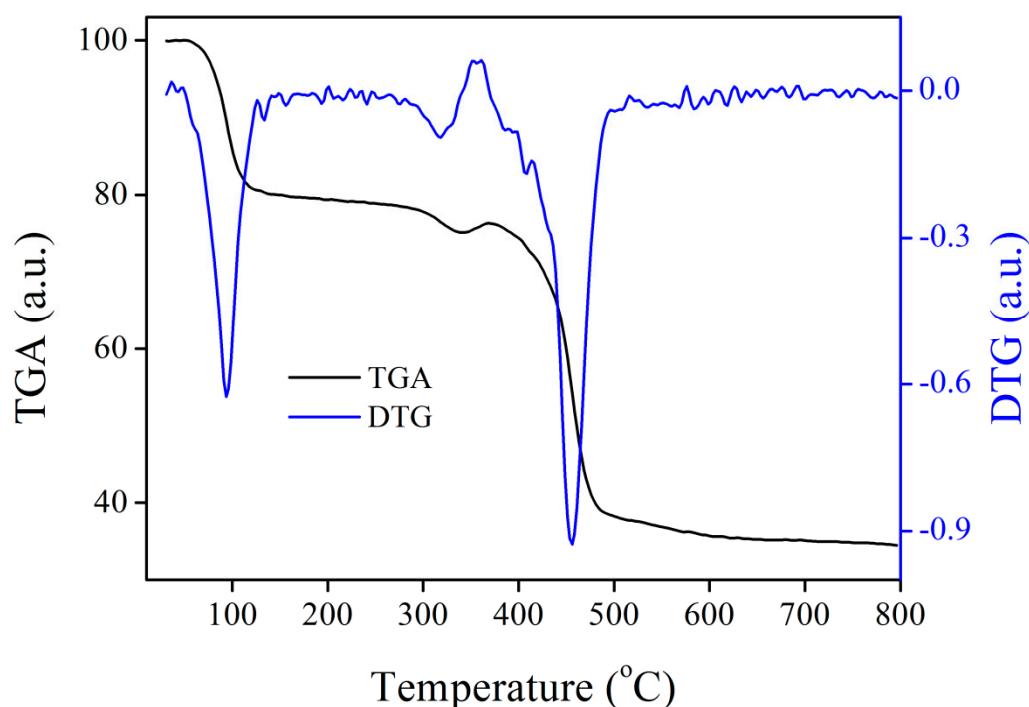


Figure 4. Thermal dynamics of RS6h@EuBTC.

Elemental analysis result of RS6h@EuBTC is compared with that of EuBTC. The C and N weight ratios are determined as 22.92% and 0.14% in EuBTC, respectively. This C weight ratio is close to its calculated value (23.12%). In the meanwhile, the material residue is responsible for the trace N content in EuBTC. After immobilizing RS6h onto EuBTC, the C and N weight ratios are increased to 32.53%, and 1.52%, respectively. Mathematically, RS6h loading level is determined as 13.3%. It is slightly lower than literature values of a hybrid structure [16].

3.1.3. Optical Characterization

RS6h@EuBTC's absorption, excitation and emission spectra are given in Figure 5. Intense UV absorption ranging from 225 nm to 340 nm is observed, showing a maximum at ~ 280 nm. This absorption band is comparable to BTC absorption [15]. It is BTC $\pi-\pi^*$ absorption of EuBTC. No absorption of rosebengal open-ring structure (~ 520 nm) is observed, indicating that nearly all RS6h molecules adopt a closed-ring structure [14]. There is weak absorption across the whole visible region from 350 nm to 700 nm. RS6h@EuBTC, thus, is a transparent suspension under daylight. RS6h@EuBTC's excitation spectrum consists of two major bands at 280 nm, and 525 nm, respectively. The first one agrees well with BTC absorption. It originates from BTC energy transfer to an emissive Eu center. There is another weak excitation band at 525 nm. This is the energy transfer from rosebengal open ring structure to the emissive Eu center. RS6h@EuBTC's emission spectrum consists of five emission bands at 541 nm, 591 nm, 615 nm, 650 nm, and 692 nm, respectively. The first one is clearly the rosebengal emission [15,16]. The following four ones agree well the characteristic Eu(III) emission bands and thus are assigned as ${}^5D_0 \rightarrow {}^7F_J$ ($J = 1,2,3,4$) transitions of Eu(III). It is clear that the electric dipole transition ${}^5D_0 \rightarrow {}^7F_2$ (615 nm) is stronger than the magnet dipole transition ${}^5D_0 \rightarrow {}^7F_1$ (591 nm). Emissive Eu(III) ions should fall in an asymmetric microenvironment in RS6h@EuBTC [17]. There is still a weak broad emission from 416 nm to 512 nm, which is ligand emission residue [17,18].

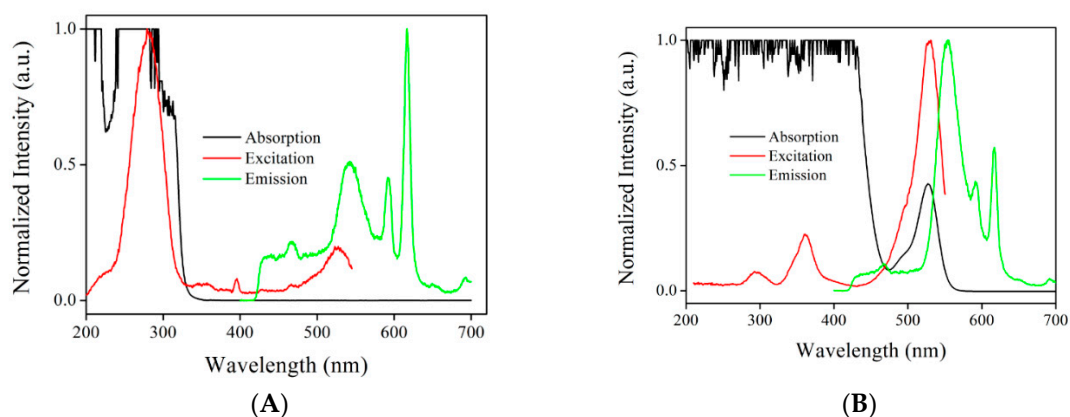


Figure 5. (A) Photophysical spectra of RS6h@EuBTC in ethanol (0.1 mg/mL); (B) Photophysical spectra of RS6h@EuBTC in ethanol (0.1 mg/mL) in the presence of TNP (100 μ M).

RS6h@EuBTC's photophysical spectra were also recorded in the presence of TNP. As depicted by Figure 5B, a broad and strong absorption (200–465 nm) covers the whole UV region and partial visible region. This strong absorption is the absorption adduct of BTC absorption (280 nm) and PA absorption (360 nm), which will be further confirmed below [17]. There is another absorption band at 527 nm. The spectral shape and wavelength are comparable to rosebengal absorption [15]. It is thus assigned as the rosebengal absorption (ring-open structure) [14,16]. This result suggests that RS6h@EuBTC begins to adopt an open-ring structure in the presence of TNP. Its possibility for TNP sensing is, hereby, confirmed. Given the increasing visible absorption, a color change will be observed, corresponding to colorimetric behavior. This hypothesis will be discussed below.

RS6h@EuBTC's excitation spectrum consists of three bands at 296 nm, 361 nm, and 528 nm, respectively. The first one is similar to RS6h@EuBTC's first excitation band (TNP-free) and thus should be BTC energy transfer to emissive Eu center. The second one (361 nm) is comparable to TNP absorption (360 nm) and consequently assigned as TNP energy transfer to an emissive Eu center [17]. The final excitation band is nearly the same as rosebengal absorption and consequently considered as rosebengal energy transfer to the emissive Eu center. Its relative intensity, compared to the BTC excitation intensity, has been greatly enhanced. It is assumed that the rosebengal molecules of RS6h@EuBTC begin to adopt an open-ring structure in the presence of TNP. These excitation bands are red shifted, compared to those in the absence of TNP. This is attributed to its electron-deficient nature. RS6h@EuBTC's emission consists of five major bands and a broad weak one, peaking at 552 nm, 592 nm, 615 nm, 650 nm and 692 nm. They are emission bands from rosebengal open-ring structure, Eu(III) and ligand, respectively. Ligand emission and Eu emission bands have been well preserved. Furthermore, the rosebengal emission band has been both, enhanced and red shifted, compared to the emission of RS6h@EuBTC. This is caused by TNP's electron-withdrawing effect. For comparison, intensity ratio $F_{552\text{ nm}}/F_{615\text{ nm}}$ is defined. Here $F_{552\text{ nm}}$ and $F_{615\text{ nm}}$ are the emission intensity values at 552 nm, and 615 nm, respectively. RS6h@EuBTC has a $F_{552\text{ nm}}/F_{615\text{ nm}}$ ratio of 1.74 in the presence of TNP, while TNP-free RS6h@EuBTC shows a four-fold smaller $F_{552\text{ nm}}/F_{615\text{ nm}}$ ratio of only 0.42. This result confirms the possibility of ratiometric sensing.

3.2. Colorimetric and Ratiometric Spectral Response

3.2.1. Colorimetric Response Based on Absorption Spectra

RS6h@EuBTC absorption spectra under increasing TNP concentrations are shown in Figure 6. TNP shows increasing absorption at 361 nm. More rosebengal molecules adopt an open-ring structure, with their absorption (528 nm) enhanced correspondingly. On the other hand, BTC π - π^* absorption (from 225 nm to 340 nm) has been well-preserved. Considering that RS6h@EuBTC's visible absorption intensity is proportional to TNP concentration, a colorimetric response may be observed. To confirm

this hypothesis, intensity ratio A/A_0 was calculated against TNP concentration (Figure 6 inset). Here parameters of A , A_0 and $[TNP]$ are the absorbance value at 528 nm, absorbance value without TNP at 528 nm, and TNP concentration, respectively. A/A_0 plots follow a linear relationship with TNP from 0 to 120 μM . The fitting equation is $A/A_0 = 33.54 + 11.36*[TNP]$, $R^2 = 0.998$. The limit of detection (LOD, $3\sigma/S$) value is observed as 1.9 μM and found to be smaller than most literature values [14,15,17–19]. Rosebengal absorption is not further increased when the TNP concentration exceed 120 μM . This indicates RS6h@EuBTC's maximum sensing capacity.

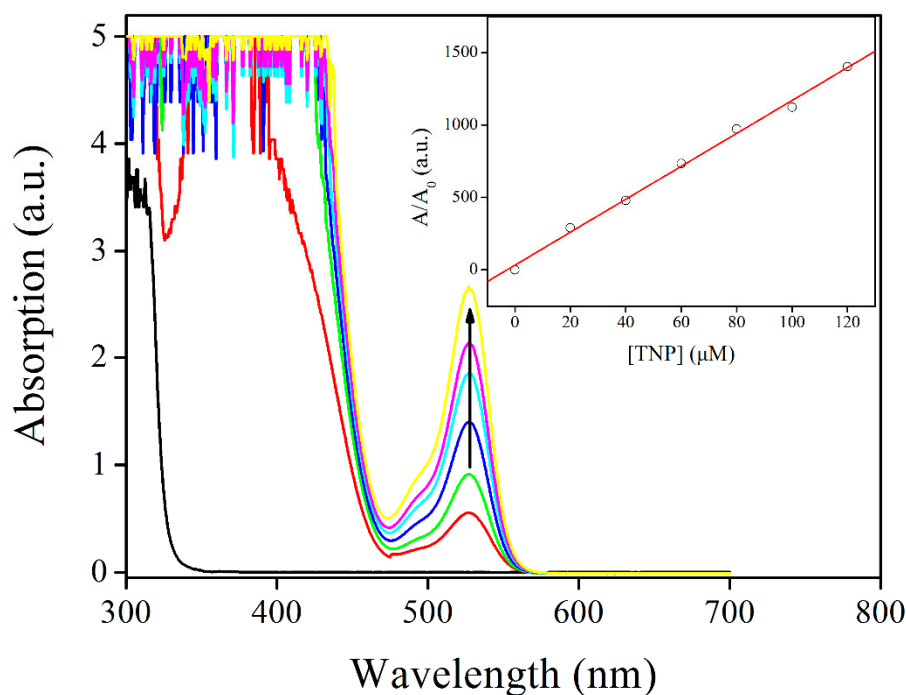


Figure 6. Absorption spectra of RS6h@EuBTC suspension in ethanol (0.1 mg/mL) under TNP concentrations from 0 to 120 μM (interval = 20 μM). Inset: A/A_0 against TNP concentration. Mean value of three test cycles was used for each data point.

3.2.2. Ratiometric Response Based on Emission Spectra

RS6h@EuBTC emission spectra under increasing TNP concentrations are shown in Figure 7. Its rosebengal emission intensity is proportional to TNP concentration. This emission is red shifted from 541 nm ($[TNP] = 0$) to 552 nm ($[TNP] = 120 \mu\text{M}$). TNP's electron-deficient structure stabilizes rosebengal emissive state and thus decreases its energy. Most Eu(III) bands (615 nm, 650 nm and 692 nm) have been well-preserved. Ratiometric sensing can be constructed with RS6h@EuBTC's rosebengal emission and Eu emission [18,19].

RS6h@EuBTC's ratiometric sensing is established using two emission bands, rosebengal emission intensity at 552 nm and Eu emission intensity at 615 nm. Intensity ratio $F_{552 \text{ nm}}/F_{615 \text{ nm}}$ is calculated against TNP concentration and shown in Figure 7 inset. Here $F_{552 \text{ nm}}$, $F_{615 \text{ nm}}$ and $[TNP]$ are the emission intensity at 552 nm, that at 615 nm and TNP concentration, respectively. $F_{552 \text{ nm}}/F_{615 \text{ nm}}$ plots follow a linear response within 0 to 120 μM . The fitting equation is $F_{552 \text{ nm}}/F_{615 \text{ nm}} = 0.55 + 0.013*[TNP]$, $R^2 = 0.997$. The LOD value ($3\sigma/S$) is observed as 4.1 μM [14,15,17–19]. This LOD value is found higher than that obtained from colorimetric sensing. This is because the low sensitivity of ratiometric sensing. Rosebengal emission is not further increased by a TNP concentration higher than 120 μM , indicating RS6h@EuBTC's maximum sensing capacity.

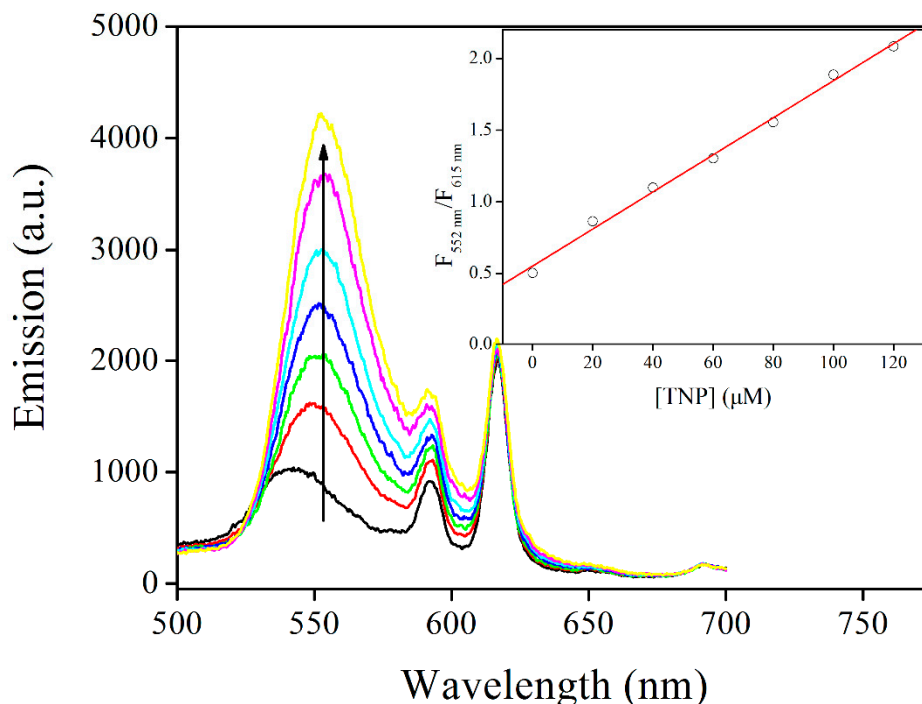


Figure 7. Emission spectra of RS6h@EuBTC suspension in ethanol (0.1 mg/mL) under TNP concentrations from 0 to 120 μM (interval = 20 μM). Inset: $F_{552\text{ nm}}/F_{615\text{ nm}}$ against TNP concentration. Mean value of three test cycles was used for each data point.

3.2.3. Instant Response and Signal Stability

In order to check the response feature towards TNP, RS6h@EuBTC emission intensity (552 nm) is continuously monitored by dropwise adding TNP into its suspension. As seen from Figure 8A, RS6h@EuBTC's rosebengal emission remains rather weak in the absence of TNP. A drop of TNP enhances its rosebengal emission greatly within only 5 s, showing a fast response. Such increasing tendency becomes smooth and then finally ceases after 25 s. A similar procedure can be fully repeated by further addition of TNP. For comparison, RS6h@EuBTC's response time is defined as the time to increase to 85% of its final intensity after each TNP addition. A short response time of 17 s is obtained. This value is much shorter than literature values of most hybrid sensing systems [19–21]. We attribute this fast response to the porous microstructure in RS6h@EuBTC which offers efficient TNP adsorption and transportation.

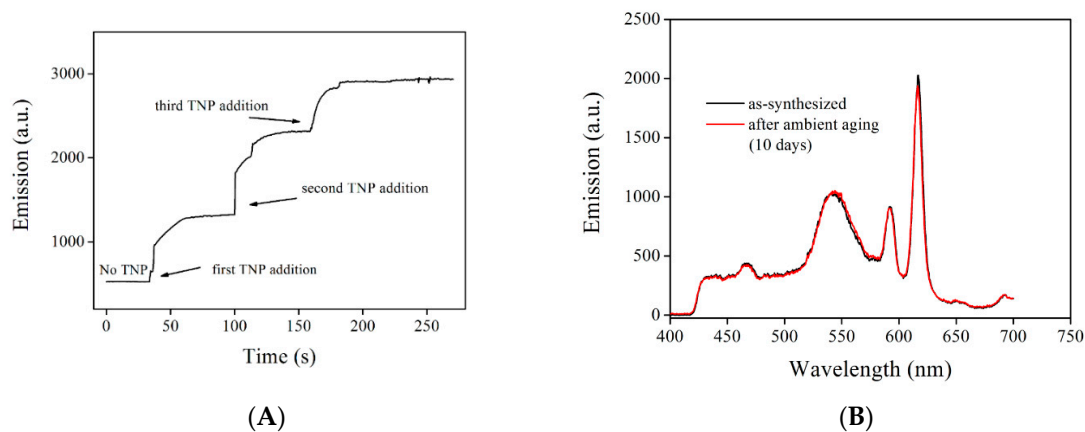


Figure 8. (A) RS6h@EuBTC emission intensity (552 nm) monitoring by dropwise addition of TNP; (B) Emission spectra of RS6h@EuBTC before and after ambient aging (10 days).

Considering that RS6h@EuBTC's ratiometric sensing is based on its emission intensity, emission stability plays an important role for sensing precision. To evaluate RS6h@EuBTC's photostability, emission spectra of fresh RS6h@EuBTC and aged RS6h@EuBTC are compared in Figure 8B. Similar emission spectra are observed, with identical emission bands and similar emission intensity values. $F_{552\text{ nm}}/F_{615\text{ nm}}$ ratio values of fresh and aged RS6h@EuBTC are calculated as 0.50, and 0.51, respectively. Although RS6h@EuBTC decreases its emission intensity slightly after aging, its $F_{552\text{ nm}}/F_{615\text{ nm}}$ ratio value (0.51) is still similar to the $F_{552\text{ nm}}/F_{615\text{ nm}}$ ratio value of fresh RS6h@EuBTC (0.50), which guarantees its sensing precision. This is the advantage of ratiometric sensing.

3.2.4. Selective Response

Generally, analyte molecules are usually dispersed in a complicated environment, loaded with competing species. A unique response towards analyte will be needed, which is also known as sensing selectivity. For a primitive evaluation on its selectivity, several interferents are added into the RS6h@EuBTC suspension. Corresponding absorption and emission spectra are shown in Figure 9. Only TNP increases RS6h@EuBTC absorption (528 nm), while the tested interferents are ineffective in doing so. This result actually confirms a good selectivity of RS6h@EuBTC's colorimetric sensing. There is neither new absorption bands nor a spectral shift, indicating that there is weak interaction between RS6h@EuBTC's rosebengal probe and these interferents. NP and Ox have more obvious effect than the others. This is because they have acidic hydrogen atoms. These released protons make rosebengal molecules take their open-ring structure [22]. Their interfering effect, however, is slim owing to their weak acidity. In this case, it is concluded that RS6h@EuBTC's colorimetric sensing has a good selectivity.

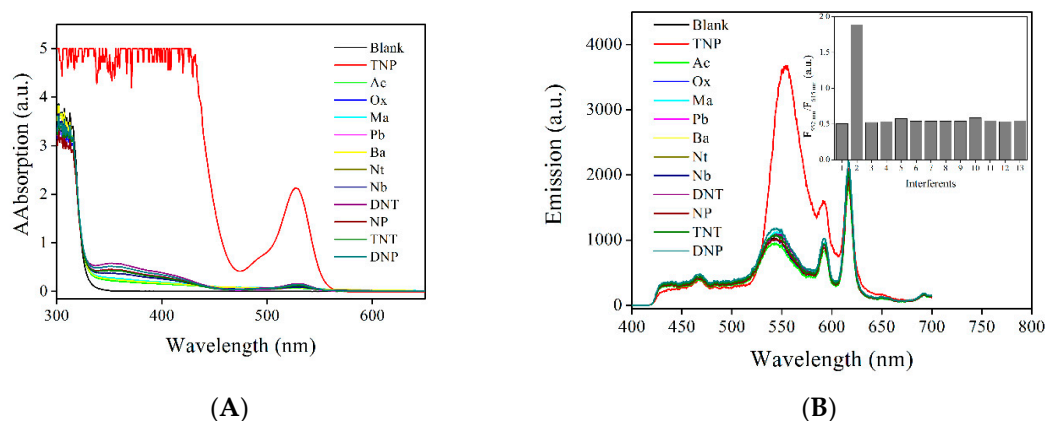


Figure 9. Absorption (A) and emission (B) spectra of RS6h@EuBTC suspension in ethanol (0.1 mg/mL) in the presence of interferents (100 μM), including Ac (acetic acid), Ox (oxalic acid), Ma (malonic acid), Pb (Phenol), Ba (benzoic acid), Nt (p-nitrotoluene), Nb (4-nitrochlorobenzene), DNT (2,4-dinitrotoluene), NP (3-nitrophenol), TNT (trinitrotoluene), DNP (2,4-dinitrophenol). Inset: $F_{552\text{ nm}}/F_{615\text{ nm}}$ ratios under interferents, 1 = blank, 2 = TNP, 3 = Ac, 4 = Ox, 5 = Ma, 6 = Pb, 7 = Ba, 8 = Nt, 9 = Nb, 10 = DNT, 11 = NP, 12 = TNT, 13 = DNP.

Figure 9B depicts RS6h@EuBTC's emission spectra for these interferents. Similar to its colorimetric sensing, RS6h@EuBTC's rhodamine emission is only enhanced by TNP. All these interferents are ineffective in so doing. Neither new emission band nor spectral shift is detected, suggesting slim interaction between sensing probe and these interferents. Similarly, NP and Ox slightly increases RS6h@EuBTC's rosebengal emission owing to their released proton. For a better evaluation, $F_{552\text{ nm}}/F_{615\text{ nm}}$ value is calculated upon these interferents. It is observed from Figure 9B inset that a high $F_{552\text{ nm}}/F_{615\text{ nm}}$ value of 1.88 is observed in the presence of TNP. These interferents, however, all have low $F_{552\text{ nm}}/F_{615\text{ nm}}$ values (<0.57). As a consequence, it is concluded that RS6h@EuBTC's ratiometric sensing also has a good selectivity.

3.2.5. Sensing Mechanism

A possible sensing procedure is proposed as follows. A TNP molecule consists of two functional fragments, which are three electron-withdrawing nitro groups and an acidic hydroxyl group. EuBTC is an electron-rich structure and may transfer its excited electrons to electron-withdrawing nitro groups, which quenches EuBTC's emission (emission turn-off). On the other hand, these nitro groups make their neighboring acidic hydroxyl group easy to release its proton, which triggers rosebengal structural transformation (closed-ring to open-ring), namely emission turn-on effect [19,21,22]. The above statement is confirmed by comparing lifetimes of RS6h@EuBTC's two emission components under various TNP concentrations. As observed from Figure 10, regardless of different TNP concentrations, both emission components follow single exponential decay pattern. Corresponding lifetimes are listed in Table 1. It is clear that rosebengal emission lifetime is prolonged from 3.29 ns at a TNP concentration of 0 μM to 5.77 ns at a TNP concentration of 120 μM . On the other hand, Eu emission lifetime is slightly quenched from 127.4 μs at a TNP concentration of 0 μM to 120.8 μs at a TNP concentration of 120 μM . This observation is consistent with RS6h@EuBTC's quenched by TNP. RS6h@EuBTC's sensing response shall be concluded as the combination of two paths. One path is rosebengal emission turn-on effect sparked by TNP proton and the other is Eu emission turn-off effect triggered by an electron transfer procedure to TNP [22,23].

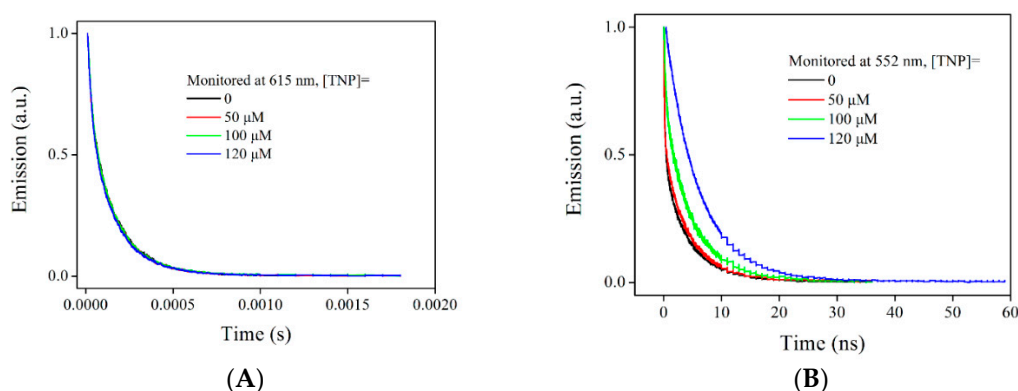


Figure 10. (A) Emission decay dynamics of RS6h@EuBTC (615 nm) under various TNP concentrations; (B) emission decay dynamics of RS6h@EuBTC (552 nm) under various TNP concentrations.

Table 1. Emission lifetimes of RS6h@EuBTC under various TNP concentrations.

TNP Concentration (μM)	0	50	100	120
552 nm (ns)	3.29	3.83	4.26	5.77
615 nm (μs)	127.4	124.9	124.1	120.8

3.3. Practical Sensing Performance

Two sensing modes and their performance, along with their sensing mechanism, have been above discussed and confirmed. Their practical sensing performance is discussed as follows. As observed from Figure 11, RS6h@EuBTC suspension is a colorless one in daylight owing to its neglectable absorption in visible region. Upon addition of TNP (20 μM), this suspension turns red-purple. Colorimetric sensing detection of RS6h@EuBTC, are thus, confirmed here. Table 2 shows the practical sensing result determined by RS6h@EuBTC's ratiometric sensing, which confirms its practicability. With the practicability confirmed above, it is safe to say that RS6h@EuBTC is superior to traditional MOF sensing materials owing to its double sensing modes. On the other hand, regardless of its good linearity, this working curve gives obvious sensing errors, owing to the limited sensitivity of this working curve.



Figure 11. RS6h@EuBTC exposed to daylight condition under no TNP (left) and TNP concentration of 20 μM (right).

Table 2. Ratiometric fluorescent sensing result of RS6h@EuBTC.

TNP Added (μM)	TNP Detected (μM)	Error
0	1.2	N/A
20	22.6	113%
50	54.6	109%
100	108.5	109%
120	125.9	105%

4. Conclusions

In summary, a rosebengal-modified nanoporous structure for TNP optical sensing was synthesized, using an organic sensitizer based on rosebengal and a supporting host of rare earth MOF. Linear response and good selectivity with a LOD of 1.9 μM were observed. Its working region was 1.9–120 μM . A short response time of 17 s was observed. This nanoporous structure was superior to traditional ones owing to its double sensing modes, absorption-based colorimetric sensing, and emission-based ratiometric sensing, respectively. The colorimetric sensing showed high sensitivity within the working region. The sensitivity of ratiometric sensing was just ~ 2.0 , but it showed good precision after being aged for 10 days. The practical sensing performance of RS6h@EuBTC was yet to be satisfied, since it tended to give positive errors. The advantage of this work is for the use of rare earth emission as an inner reference to construct ratiometric sensing. However, there are problems to be solved. Future effort should be devoted to broaden sensing region and the sensitivity of ratiometric fluorescent sensing.

Author Contributions: Conceptualization, K.S. and L.G.; methodology, H.Y. and J.Z.; formal analysis, Y.B. and Y.G.; data curation, J.Y.; writing—original draft preparation, K.S. All authors have read and agreed to the published version of the manuscript.

Funding: This research was financially supported by the National Natural Science Foundation of China, grant number 31870486, Natural Science Foundation of Jilin Province, grant number No.JJKH20170657KJ and the Natural Science Foundation of Changchun Normal University, grant number 201606, 2017017.

Conflicts of Interest: The authors declare no conflict of interest.

References

- Nagarkar, S.S.; Desai, A.V.; Ghosh, S.K. Engineering metal–organic frameworks for aqueous phase 2, 4, 6-trinitrophenol (TNP) sensing. *CrystEngComm* **2016**, *18*, 2994–3007. [[CrossRef](#)]
- Chopra, R.; Bhalla, V.; Kumar, M.; Kaur, S. Rhodamine appended hexaphenylbenzene derivative: Through bond energy transfer for sensing of picric acid. *RSC Adv.* **2015**, *5*, 24336–24341. [[CrossRef](#)]
- Shanmugaraju, S.; Mukherjee, P.S. π -Electron rich small molecule sensors for the recognition of nitroaromatics. *Chem. Commun.* **2015**, *51*, 16014–16032. [[CrossRef](#)] [[PubMed](#)]

4. Joarder, B.; Desai, A.V.; Samanta, P.; Mukherjee, S.; Ghosh, S.K. Selective and Sensitive Aqueous-Phase Detection of 2, 4, 6-Trinitrophenol (TNP) by an Amine-Functionalized Metal–Organic Framework. *Chemistry* **2015**, *21*, 965–969. [[CrossRef](#)] [[PubMed](#)]
5. Walsh, M.E. Determination of nitroaromatic, nitramine, and nitrate ester explosives in soil by gas chromatography and an electron capture detector. *Talanta* **2001**, *54*, 427–438. [[CrossRef](#)]
6. Sylvia, J.M.; Janni, J.A.; Klein, J.D.; Spencer, K.M. Surface-enhanced Raman detection of 2, 4-dinitrotoluene impurity vapor as a marker to locate landmines. *Anal. Chem.* **2000**, *72*, 5834–5840. [[CrossRef](#)]
7. Germain, M.E.; Knapp, M.J. Optical explosives detection: From color changes to fluorescence turn-on. *Chem. Soc. Rev.* **2009**, *38*, 2543–2555. [[CrossRef](#)]
8. Nagarkar, S.S.; Joarder, B.; Chaudhari, A.K.; Mukherjee, S.; Ghosh, S.K. Highly selective detection of nitro explosives by a luminescent metal–organic framework. *Angew. Chem. Int. Ed.* **2013**, *52*, 2881–2885. [[CrossRef](#)]
9. Zhao, S.N.; Song, X.Z.; Zhu, M.; Meng, X.; Wu, L.L.; Feng, J.; Song, S.Y.; Zhang, H.J. Encapsulation of Ln III Ions/Dyes within a Microporous Anionic MOF by Post-synthetic Ionic Exchange Serving as a Ln III Ion Probe and Two-Color Luminescent Sensors. *Chemistry* **2015**, *21*, 9748–9752. [[CrossRef](#)]
10. Campagnol, N.; Souza, E.R.; de Vos, D.E.; Binnemans, K.; Fransaer, J. Luminescent terbium-containing metal–organic framework films: New approaches for the electrochemical synthesis and application as detectors for explosives. *Chem. Commun.* **2014**, *50*, 12545–12547. [[CrossRef](#)]
11. Zhang, Y.; Li, B.; Ma, H.; Zhang, L.; Zheng, Y. Rapid and facile ratiometric detection of an anthrax biomarker by regulating energy transfer process in bio-metal-organic framework. *Biosens. Bioelectron.* **2016**, *85*, 287–293. [[CrossRef](#)]
12. Dong, M.J.; Zhao, M.; Ou, S.; Zou, C.; Wu, C.D. A luminescent dye @ MOF platform: Emission fingerprint relationships of volatile organic molecules. *Angew. Chem., Int. Ed.* **2014**, *53*, 1575–1579. [[CrossRef](#)]
13. Cui, Y.; Song, R.; Yu, J.; Liu, M.; Wang, Z.; Wu, C.; Yang, Y.; Wang, Z.; Chen, B.; Qian, G. Dual-emitting MOF \cap dye composite for ratiometric temperature sensing. *Adv. Mater.* **2015**, *27*, 1420–1425. [[CrossRef](#)]
14. Wang, Y.H.; Li, B.; Zhang, L.M.; Liu, L.N.; Zuo, Q.H.; Li, P. A highly selective regenerable optical sensor for detection of mercury (II) ion in water using organic–inorganic hybrid nanomaterials containing pyrene. *New J. Chem.* **2010**, *34*, 1946–1953. [[CrossRef](#)]
15. Liu, K.; You, H.; Zheng, Y.; Jia, G.; Zhang, L.; Huang, Y.; Yang, M.; Song, Y.; Zhang, H. Facile shape-controlled synthesis of luminescent europium benzene-1,3,5-tricarboxylate architectures at room temperature. *CrystEngComm* **2009**, *11*, 2622–2628. [[CrossRef](#)]
16. Wen, Y.; Cheng, J.; Feng, Y.; Zhang, J.; Li, Z.; Yao, Y. Yao. *Chin. J. Struct. Chem.* **2005**, *24*, 1440.
17. Zhang, L.; Li, B. A series of Eu (III) emitters with a novel triphenylamine-derived beta-diketone ligand. *J. Lumin.* **2009**, *129*, 1304–1308. [[CrossRef](#)]
18. Xiao, J.D.; Qiu, L.G.; Ke, F.; Yuan, Y.P.; Xu, G.S.; Wang, Y.M.; Jiang, X. Rapid synthesis of nanoscale terbium-based metal–organic frameworks by a combined ultrasound–vapour phase diffusion method for highly selective sensing of picric acid. *J. Mater. Chem. A* **2013**, *1*, 8745–8752. [[CrossRef](#)]
19. Gole, B.; Bar, A.K.; Mukherjee, P.S. Modification of extended open frameworks with fluorescent tags for sensing explosives: Competition between size selectivity and electron deficiency. *Chemistry* **2014**, *20*, 2276–2291. [[CrossRef](#)]
20. Song, X.Z.; Song, S.Y.; Zhao, S.N.; Hao, Z.M.; Zhu, M.; Meng, X.; Wu, L.L.; Zhang, H.J. Single-Crystal-to-Single-Crystal transformation of a europium (III) metal–organic framework producing a multi-responsive luminescent sensor. *Adv. Funct. Mater.* **2014**, *24*, 4034–4041. [[CrossRef](#)]
21. Khatua, S.; Goswami, S.; Biswas, S.; Tomar, K.; Jena, H.S.; Konar, S. Stable multiresponsive luminescent MOF for colorimetric detection of small molecules in selective and reversible manner. *Chem. Mater.* **2015**, *27*, 5349–5360. [[CrossRef](#)]
22. Mostakim, S.K.; Biswas, S. A thiadiazole-functionalized Zr (IV)-based metal–organic framework as a highly fluorescent probe for the selective detection of picric acid. *CrystEngComm* **2016**, *18*, 3104–3113.
23. Hu, X.L.; Qin, C.; Wang, X.L.; Shao, K.Z.; Su, Z.M. A luminescent dye@ MOF as a dual-emitting platform for sensing explosives. *Chem. Commun.* **2015**, *51*, 17521–17524. [[CrossRef](#)]

